



The chemical modification of graphene antidot lattices

Di Wu^a, Zhiming Yu^b, Jin Xiao^a, Fangping Ouyang^{a,c,*}

^a School of Physics Science and Technology, Central South University, Changsha 410083, PR China

^b School of Material Technology and Engineering, Central South University, Changsha 410083, PR China

^c College of Chemistry and Molecular Engineering and Beijing National Laboratory for Molecular Sciences, Peking University, Beijing 100871, PR China

ARTICLE INFO

Article history:

Received 18 March 2010

Received in revised form

7 June 2010

Accepted 15 June 2010

Available online 19 June 2010

ABSTRACT

By first-principles calculations, the electronic properties of chemical modified graphene antidot lattices with hexagonal holes (HexGALs) were investigated. The modified HexGALs adsorbed by carboxyl and amino groups, the vacancy defected HexGALs by removing carbon atoms and the doped HexGALs substitutionally by boron and nitrogen were all studied. It was found that the adsorptions of carboxyl or amino groups on HexGALs cannot lead to the transition from intrinsic semiconductor to p-type or n-type, but can induce the magnetism to nonmagnetic HexGALs in the case of the imbalance adsorption of groups on two sublattices, which is very similar with the case of corresponding vacancy defected HexGALs. But the adsorptions of the second carboxyl and amino tend to kill the magnetism. On the contrary, the substitutional doping of boron and nitrogen in HexGALs cannot induce magnetism but can turn HexGALs to expected p-type and n-type semiconductor, respectively. The appearance of the net magnetism is closely related with the number difference of carbon atoms of two sublattices in the π conjugation network.

© 2010 Elsevier B.V. All rights reserved.

1. Introduction

Graphene, combining a high mobility ($\sim 15\,000\text{ cm}^2/\text{V s}$) with the possibility of patterning using e-beam lithography, attracts more and more attentions from its discovery [1–4]. However, the perfect graphene is semimetallic and thus not suitable for many electronic and optoelectronic applications which require gapped semiconductor material. For opening the gap of graphene at the room temperature, patterning graphene into nanoribbons by e-beam lithography [4], chemical method [5] and unzipping carbon nanotubes [6, 7] has been realized, as well as tuning the gap of bilayer graphene by double gate [8]. Alternatively, graphene antidot lattices (GALs), a periodic array of holes (antidots) on graphene, are theoretically predicted a very promising material for their excellent properties of turning the semimetallic graphene into a gapped semiconductor, and the size of the gap can be tuned via the antidot lattice parameters. Moreover, the GALs with some special shapes of antidots can act as a magnetic superatoms [9–16]. Recent experimental investigations, using e-beam lithography [17], oxygen plasma treatment [18], transmission electron microscope [19] and bottom-up synthesis [20] to create antidots in graphene, suggest that it is

possible to employ such techniques to create variable-sized graphene antidots.

It has been demonstrated theoretically and experimentally that carboxyl (amino) adsorbed and boron (nitrogen) doped graphene and graphene nanoribbons are p-type (n-type) conductivity [21–24]. Moreover, carboxyl functionalized carbon materials can be further functionalized through derived carboxyl with other chemical moieties, such as amide, ester bonds and so on [25,26], which makes it potential applications on biological molecule detecting. On the other hand, the chemical contamination is inevitable more or less in the manufacture process of GALs. So investigating the influence of chemical modification on the electronic properties of GALs is fairly necessary.

In our work, the influences of carboxyl and amino groups adsorbed on GAL with hexagonal holes (HexGAL) were mainly studied by first-principles calculations, as well as the case of boron and nitrogen doped HexGAL. And we compared them with the case of vacancy defected HexGALs which is achieved by removing the carbon atoms at the adsorptive or doped sites. Some interesting and valuable results were obtained.

2. Computational method

The calculations were performed by the Vienna Ab initio Simulation Package (VASP) [27], which is based on density functional theory and plane-wave pseudopotential method. The plane-wave cutoff energy was 400 eV for all calculations. The

* Corresponding author at: School of Physics Science and Technology, Central South University, Changsha 410083, PR China. Tel./fax: +86 731 82539729.

E-mail address: ouyangfp06@tsinghua.org.cn (F. Ouyang).

generalized gradient approximation (GGA) [28] and the Perdew-Burke-Ernzerhof (PBE) exchange-correlation function [29] was chosen. All the atomic structures were fully optimized using the conjugate gradient algorithm until the residual forces was smaller than 0.01 eV/\AA and the change of total energy was smaller than 10^{-4} eV . All geometry optimizations and electronic structure calculations were performed using periodic boundary conditions, and the brillouin-zone integrations were performed using an $11 \times 11 \times 1$ Monkhorst-Pach (MP) grid [30]. To avoid the interaction between adjacent graphene layers, each graphene plane was separated by greater than 10 \AA of vacuum.

3. Results and discussion

The unit cell of HexGAL investigated in our calculations is shown in Fig. 1b, which, including 48 carbon atoms, is obtained through

extracting six carbon atoms from the centre of perfect graphene supercell (Fig. 1a). All the suspended bonds at the edge of antidot were saturated with hydrogen. The periodic array of hexagonal unit cell of HexGAL results in a rhombic antidot lattice (Fig. 1c) and the base vectors were denoted by \mathbf{a}_1 and \mathbf{a}_2 , whose magnitudes are both 12.816 \AA . After geometry optimization, the lengths of C–C bonds at the edge of antidot change to 1.392 \AA from the original 1.424 \AA of perfect graphene, and the length of C–H bond is 1.091 \AA .

From the corresponding band spectra of perfect graphene (Fig. 1a) and HexGAL (Fig. 1b), It can be seen that the perturbation of periodic antidots removes the bands degeneracy at Γ points and results in an energy gap (0.8088 eV), because the antidots partly destroy the π conjugation network in graphene and the narrow connecting branches between the antidots behave as a network of nanoribbons [17]. Because the removal of six symmetrical carbon atoms at the centre of graphene supercell does not induce the imbalance of graphene sublattices, so the

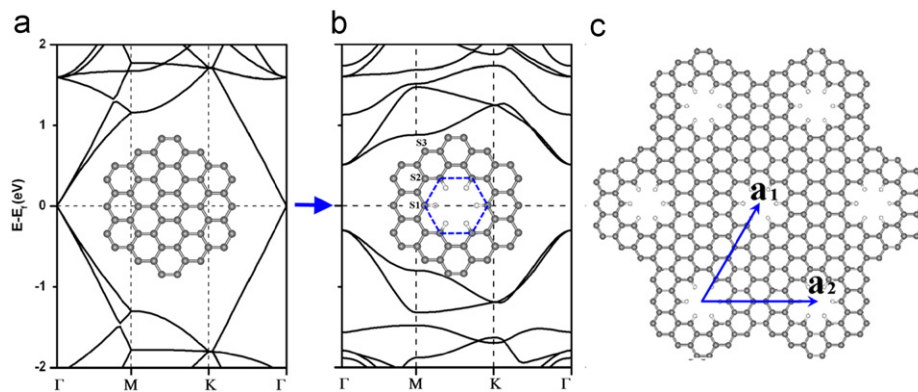


Fig. 1. The band structures of (a) graphene and (b) HexGAL. The insets are the corresponding supercells. (c) Rhombic antidot lattice of HexGAL.

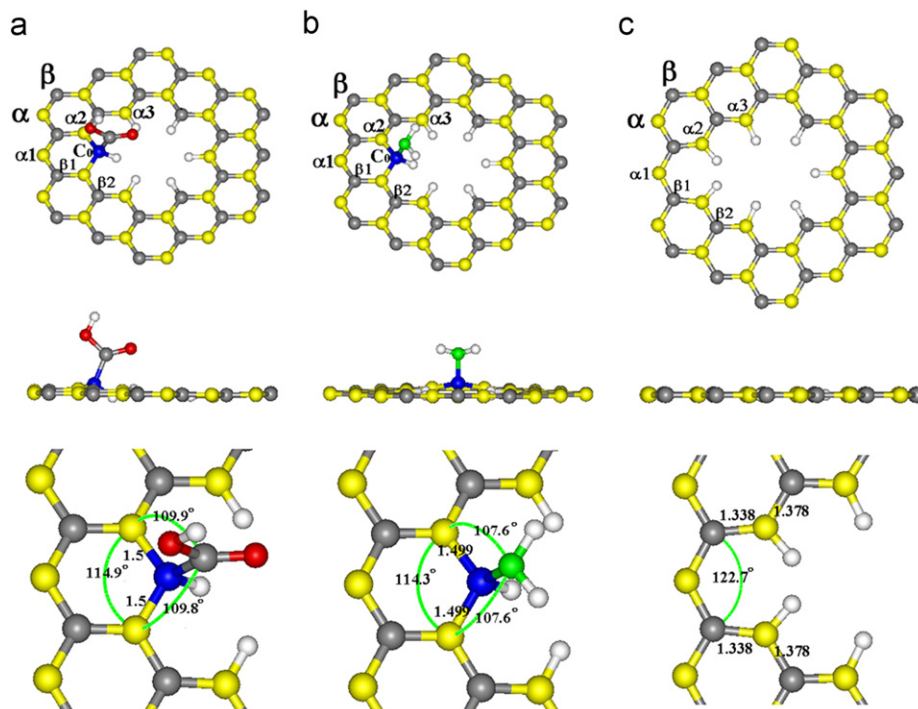


Fig. 2. The tilt view (upper panel), side view (middle panel) and geometry parameters (lower panel) around C_0 of (a) carboxyl adsorbed HexGAL, (b) amino adsorbed HexGAL and (c) vacancy defected HexGAL. The color code: yellow, carbon in α -sublattice; Grey, carbon in β -sublattice; blue, C_0 at the adsorptive site; red, oxygen; green, nitrogen; white, hydrogen. (For interpretation of the references to color in this figure legend, the reader is referred to the web version of this article.)

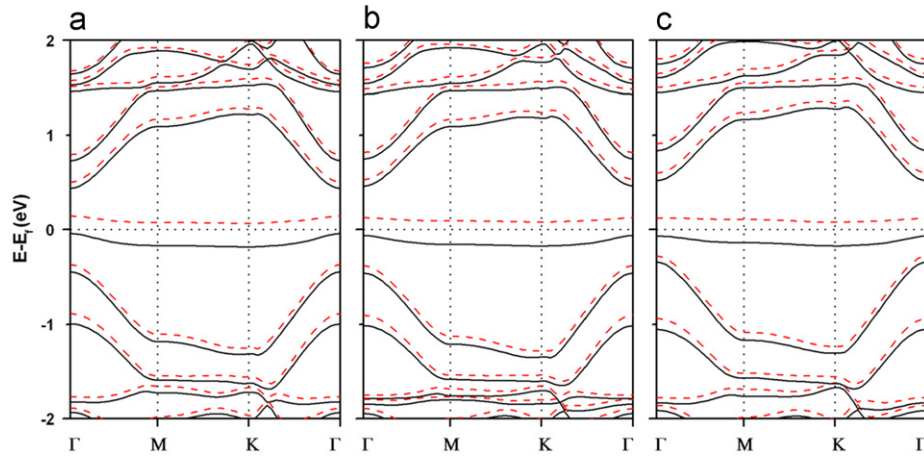


Fig. 3. The spin-polarized band structures of (a) carboxyl HexGAL, (b) amino HexGAL and (c) vacancy defected graphene. The black solid lines represent spin-up bands and the red dashed lines represent spin-down bands. The fermi level is set to zero and is denoted by dotted line. (For interpretation of the references to color in this figure legend, the reader is referred to the web version of this article.)

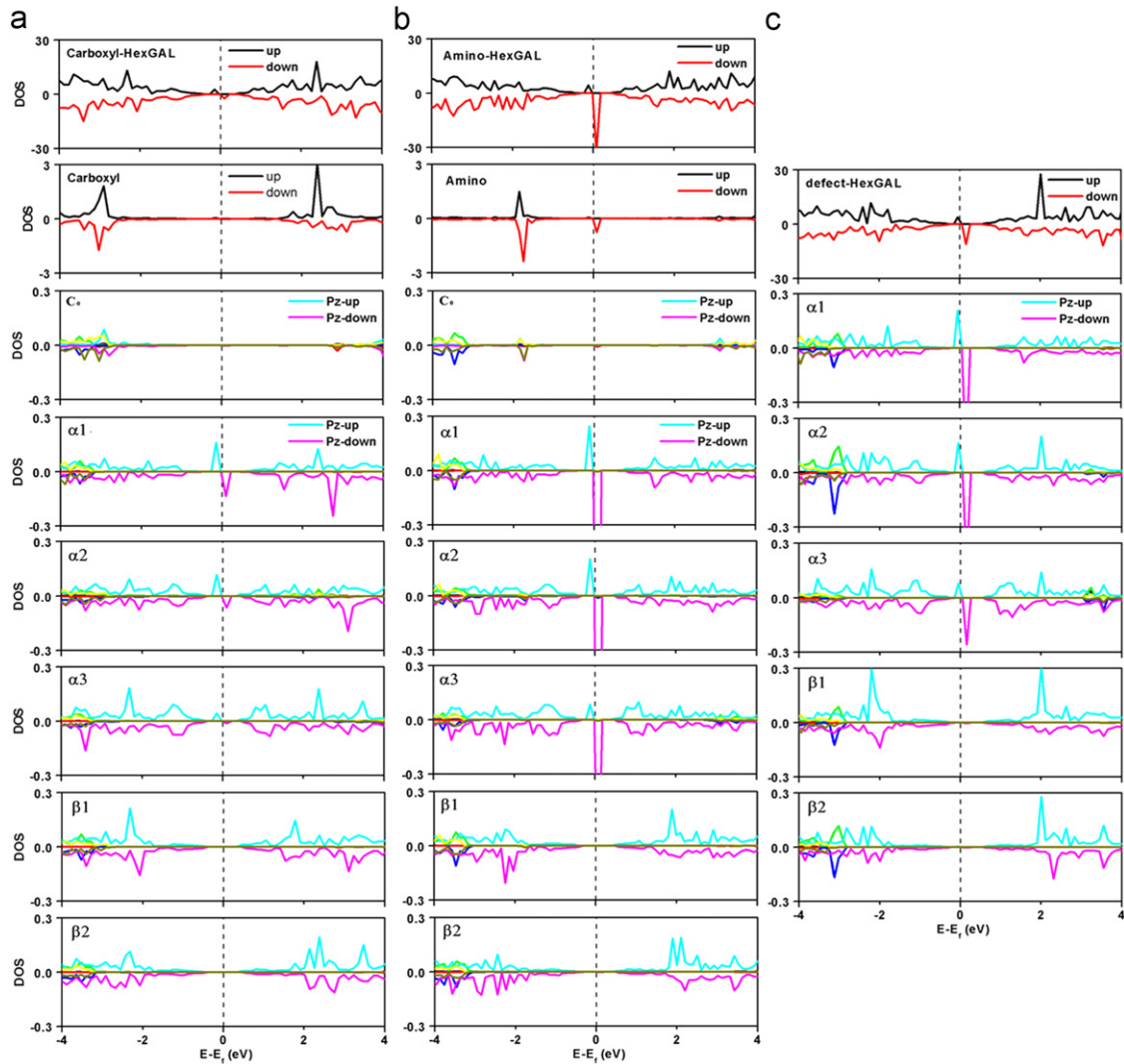


Fig. 4. The TDOS (upper panel) and PDOS (lower middle panel) spectra of Carboxyl HexGAL (a), amino HexGAL (b) and vacancy defected HexGAL (c). The black upward and red downward lines in TDOS represent spin-up and spin-down states, respectively. The cyan upward and pink downward lines in PDOS represent spin-up and spin-down states of Pz orbital electrons, respectively. Other colors in PDOS represent the spin-polarized states of other orbital electrons. The positions of α_1 , α_2 , α_3 , β_1 , β_2 and C_0 carbons are marked in Fig. 2. (For interpretation of the references to color in this figure legend, the reader is referred to the web version of this article.)

HexGAL are still nonmagnetic. This is coincident with Refs. [9,12,31] calculated by tight binding model.

3.1. The electronic properties of modified HexGAL with single defect per unit cell

Three types of defects in HexGAL were taken into consideration: Carboxyl adsorbed defect, amino adsorbed defect and vacancy defect. Calculations indicate that the energetically favorable site for three types of single defect are all located at the edge of antidots, as is in accordant with Refs. [21,26] in which the carboxyls usually appear at the defect or the edge of graphene. The six equivalent high-active sites at the edge of antidots construct a hexagonal antidot, which is marked by blue dashed hexagon in Fig. 1b.

Fig. 2 shows the unit cells of (a) single carboxyl adsorbed, (b) single amino adsorbed HexGAL and (c) single vacancy defected HexGAL. From the top to the bottom, the illustrations are, respectively, the tilt views, the side views and the geometry around defects. The yellow, grey and blue balls represent the carbon atoms in α -sublattice, in β -sublattice and at the adsorptive sites (C_0), respectively. The red, green and white balls represent oxygen, nitrogen and hydrogen atoms, respectively. It is obvious that the blue carbon C_0 at the adsorptive site is higher than the surface of HexGAL (see the middle panel of Figs. 2a and b), and its C–C bonds connected with adjacent carbons change to 1.500 Å for carboxyl HexGAL and 1.499 Å for amino HexGAL from original 1.394 Å. The angle between these two bonds changes to 114.9° for carboxyl HexGAL and 114.3° for amino HexGAL from original 122.8° (see the lower panel of Fig. 2a and b). Fig. 2c is the case of corresponding vacancy defected HexGAL achieved by removing C_0

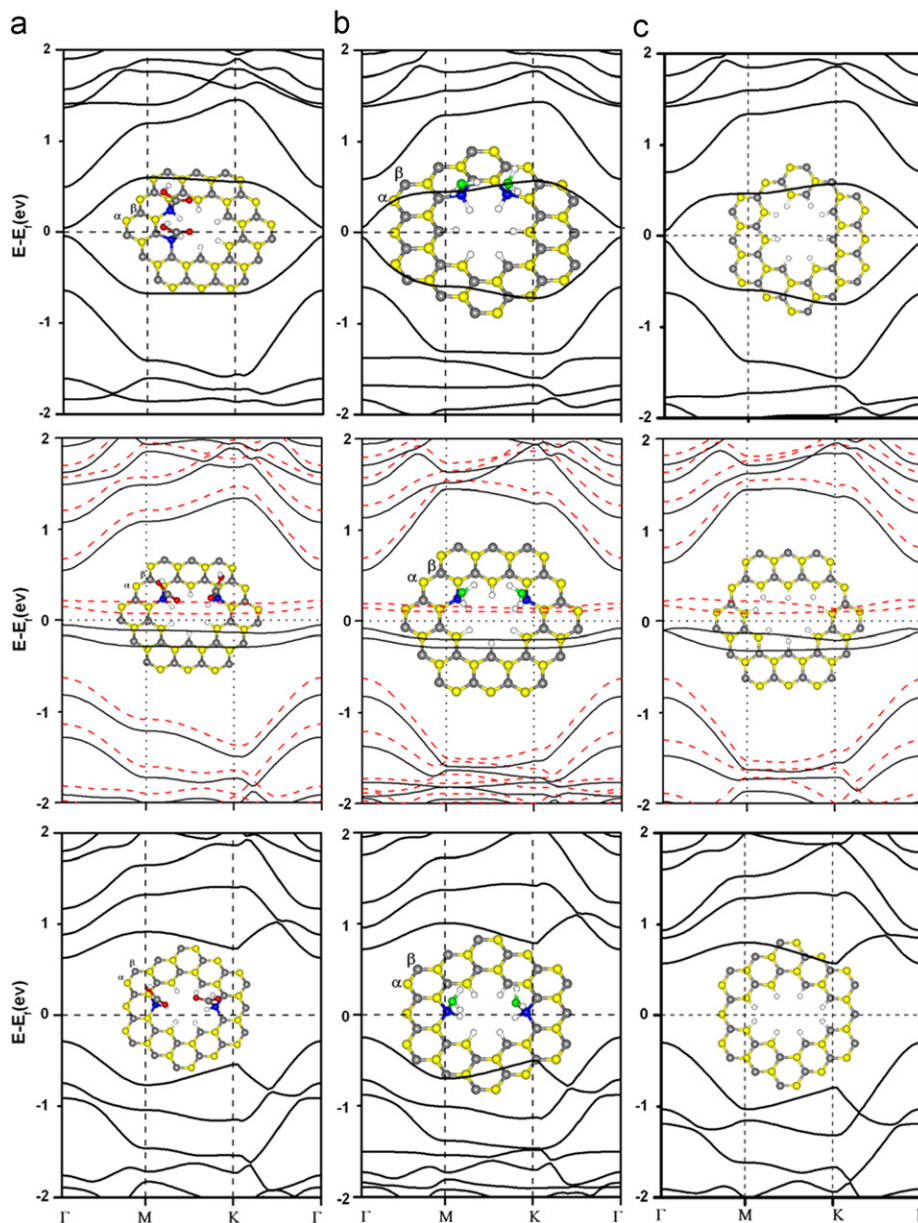


Fig. 5. The band structures of (a) double carboxyl adsorbed HexGAL, (b) double amino adsorbed HexGAL and (c) double vacancy defected HexGAL at ortho- (upper panel), meta- (middle panel) and para-position (lower panel), respectively. The insets are the corresponding atomic structures. Color code: yellow, carbon in α -sublattice; grey, carbon in β -sublattice; blue, C_0 at the adsorptive site; Red, oxygen; green, nitrogen; white, hydrogen. (For interpretation of the references to color in this figure legend, the reader is referred to the web version of this article.)

at the chemisorption site, which results in the angle at the opposite corner of the missing carbon enlarging to 122.7° , while all the carbon atoms are still located in the same plane.

The spin-polarized band structures of carboxyl adsorbed, amino adsorbed and vacancy defected HexGAL for one defect per unit cell are shown in Fig. 3(a)–(c), respectively. The solid black lines and dashed red lines correspond to the spin-up bands and spin-down bands, respectively. Though the carboxyl and amino are generally viewed as electron acceptor and electron donor, respectively, the adsorptions of them on HexGALs do not lead to p-type and n-type conductivity. On the contrary, the band spectra of carboxyl HexGAL (Fig. 3a) and amino HexGAL (Fig. 3b) are very similar, and are nearly the same with that of the vacancy defected HexGAL (Fig. 3c). All three types of single defects per unit cell lead to the appearances of a pair of spin-polarized quasi-flat bands near the fermi level, in which the spin-up band is filled while the spin-down band is empty, thus $1\mu\text{B}$ magnetic moment per unit cell appears.

For clarifying the distribution of these quasilocalized states, the total and partial density of states (TDOS and PDOS) of carboxyl HexGAL, amino HexGAL and vacancy defected HexGAL are shown in Fig. 4(a–c), respectively. The black upward lines and red downward lines represent the spin-up and spin-down states, respectively. In the TDOS spectra of defected HexGAL (the top panel), a pair of strong peak appears near fermi level, and the spin-up state is filled and the spin-down state is empty. But in the PDOS spectra (the upper middle panel in Fig. 4a and b) of carboxyl, amino and C_0 atoms (carbon atoms at the adsorptive site), there are no obvious signal near fermi level, even near the bottom of conduction band and the top of valence band, which implies that the π conjugation network of HexGAL is interrupted at C_0 position. This is coincidence with the hybrid orbitals transition of the adsorbed carbon from sp^2 to sp^3 induced by the chemisorption. The chemisorption defects of carboxyl HexGAL and amino HexGAL result in the removal of one carbon atom from the π conjugation network, which has the equivalent effect with the vacancy defect of HexGAL for the electronic structure. This result is fairly similar with that of Refs. [11,31,32] calculated by tight binding model, but the imbalance of sublattices in their results is not induced by an adsorption but by the vacancy defect or different shapes of antidot.

Several typical PDOS spectra of other carbon atoms in three types of defected HexGAL are shown in the lower middle panel of Fig. 4, and the corresponding carbon position in three defected HexGALs are labeled in Fig. 2. The cyan upward lines and pink downward lines represent the spin-up and spin-down states of P_z orbitals, respectively, and other color lines represent spin polarized states of three sp^2 hybrid orbitals. It is obvious that the states near the bottom of conduction band and the top of valence band for three types of defected HexGAL are all occupied by P_z electrons of all the atoms except for the adsorbed carbon and adsorbate, whereas the TDOS strong peak near fermi level are formed only by the states of P_z electrons of α -carbons. Also, in all PDOS spectra of α -carbons, the spin-up state near fermi level is

Table 1
The binding energy of the second carboxyl and amino adsorbed on HexGAL (eV)^a.

	Ortho-position	Meta-position	Para-position
Carboxyl	−1.6151	−1.0375	−1.7727
Amino	−1.9864	−1.1741	−2.0053

^a The binding energy E_b is defined as $E_b = E_{\text{double-adsorbed HexGAL}} - E_{\text{group}} - E_{\text{single-adsorbed HexGAL}}$, in which $E_{\text{double-adsorbed HexGAL}}$ is the total energy of double carboxyl or amino adsorbed HexGAL, E_{group} is the energy of carboxyl or amino and $E_{\text{single-adsorbed HexGAL}}$ is the total energy of single carboxyl or amino adsorbed HexGAL.

filled and the spin-down state is empty. That is to say the magnetism of single defected HexGAL is distributed only on the α -sublattice. Carefully examining the peak amplitude of α -carbon PDOS at fermi level, we also found that the peak amplitude decreases with the increase of distance between the considered carbon and the defect, which suggests that the magnetism of HexGAL is mainly distributed on α -carbons around the defect.

3.2. The electronic properties of modified HexGAL with two defects per unit cell

Because of the high chemical activity of carbons at the antidot edge of HexGAL, the electronic structures of two carboxyl adsorbed HexGAL, two aminos adsorbed HexGAL and two vacancy defected HexGAL with the defects at the antidot edge were investigated also. The corresponding band structures are shown in Fig. 5(a–c), and the insets are the corresponding atomic structures. Since the six equivalent carbon atoms at the antidot edge construct a hexagon (see Fig. 1b), there are three different chemisorptive or vacancy defected geometries for two defects per unit cell: ortho- (upper panel), meta- (middle panel) and para-position (lower panel) defected geometries. It is obvious that for the same geometries of different defects, the band structures are very similar, which also indicates that the chemisorption defects are equivalent with the corresponding vacancy defects. However, for the ortho- and para-defected HexGALs (upper and lower panel in Fig. 5), there are no local energy levels at fermi level, whereas the band spectra of meta-defected HexGALs have two pair of spin-polarized bands near fermi level (middle panel in Fig. 5), in which two spin-up bands are filled and two spin-down bands are empty, thus $2\mu\text{B}$ magnetic moment per unit cell is induced.

The graphene lattice is the bipartite lattice, which can be viewed as two interpenetrating hexagonal sublattices of carbon atoms (labeled α and β). For the perfect HexGAL, the two sublattices are equivalent and there is no magnetism. When single carboxyl or amino group adsorbed at a carbon or a carbon was removed per unit cell, only one carbon atom is removed from the π conjugation network of HexGALs, resulting in a number difference of one carbon atom between two sublattices in the π conjugation network and inducing $1\mu\text{B}$ magnetic moment per unit cell. But for three types of defected HexGALs with two defects per unit cell, the ortho- and para-defected HexGALs all have the same carbon number in two sublattices though two carbon atoms

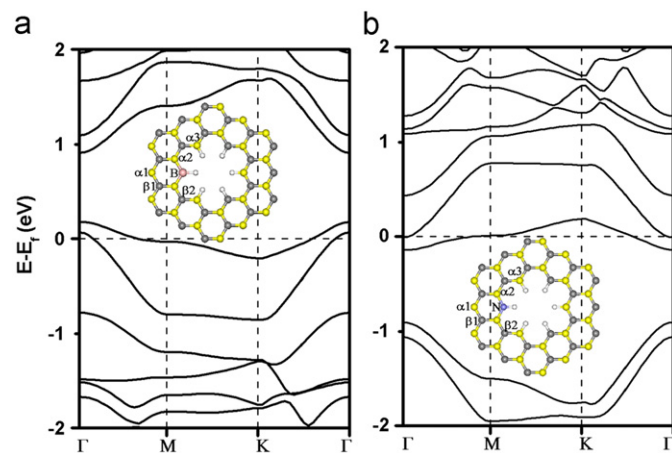


Fig. 6. The band structures and unit cells (insets) of the doped HexGALs by (a) boron and (b) nitrogen substitutionally. Color code: yellow, carbon in α -sublattice; grey, carbon in β -sublattice; pink, boron; purple, nitrogen; white, hydrogen. (For interpretation of the references to color in this figure legend, the reader is referred to the web version of this article.)

are removed from the π conjugation network, because these two carbon atoms belong to different sublattices. However, for the meta-defected HexGALs, two carbons removed from the π conjugation network belong to the same sublattice, which result in a number difference of two carbon atoms between two sublattices in the π conjugation network and induce $2\mu\text{B}$ magnetic moment per unit cell. That is to say, for hydrogen saturated HexGAL, the sublattice imbalance of defected HexGAL can induce $|n_\alpha - n_\beta|\mu\text{B}$ magnetic moment per unit cell, in which n_α and n_β are, respectively, the carbon number of two sublattices in the π conjugation network.

Through calculating the binding energy (listed in Table 1) of the second carboxyl and amino adsorbed on HexGAL, we found that the most energetically stable site for the second group is the para-adsorption, which implies that the magnetic chemisorption defect on HexGAL is unstable, and the adsorption of the second carboxyl or amino tends to kill the magnetism and recovers the

magnetic moment to zero. This property is the same with the case of hydrogen adsorbed graphene [33].

3.3. The electronic properties of doped HexGAL by boron and nitrogen

The electronic properties of the doped HexGAL substitutionally by boron and nitrogen were also studied. Several nonequivalent doping sites are still at the edge of HexGAL. Fig. 6 is the band structures of the doped HexGAL, respectively, by boron (a) and nitrogen (b) at the antidot edge. In opposition to the case of chemisorption HexGAL, boron and nitrogen doping in HexGAL cannot induce magnetism to HexGAL but result in p-type and n-type semiconductors, respectively. Fig. 7 is the TDOS (upper panel) and PDOS (lower middle panel) of the doped HexGAL,

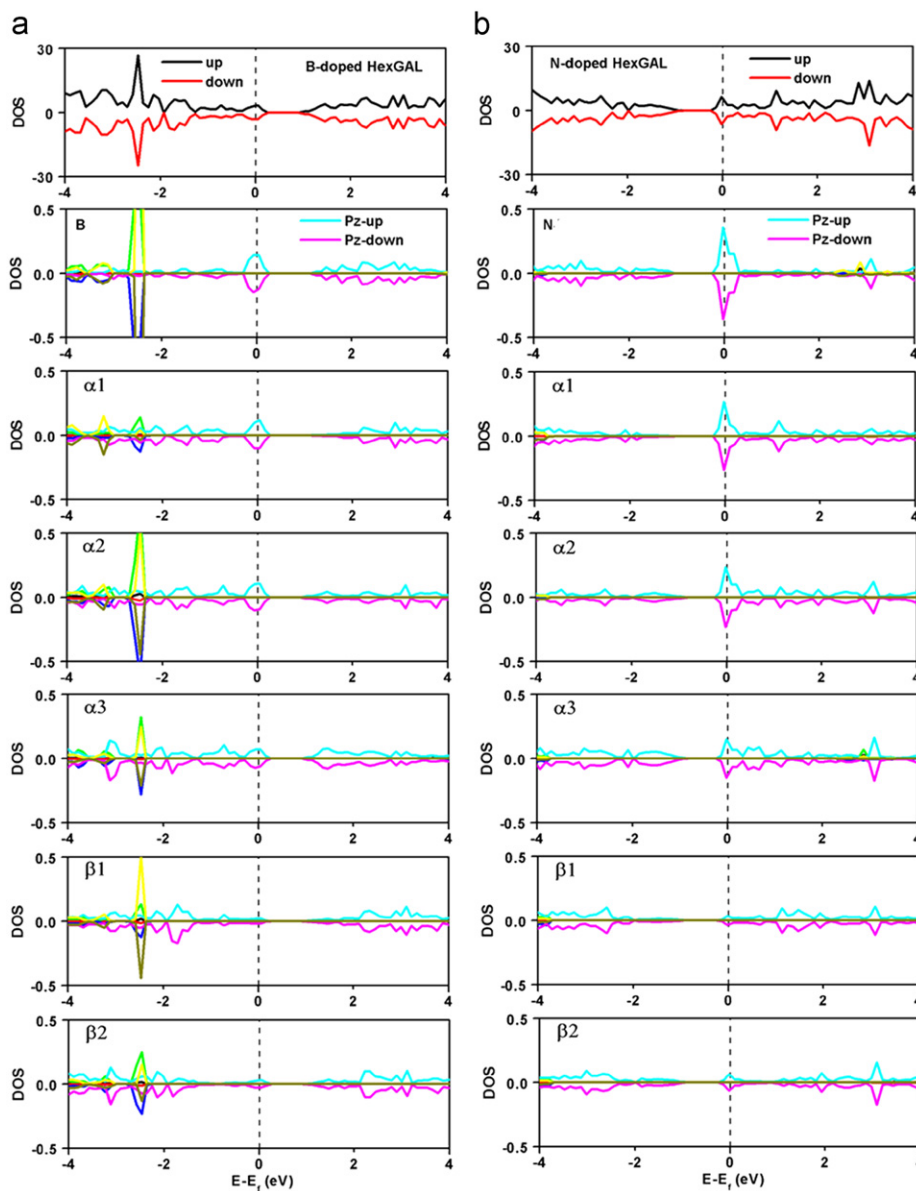


Fig. 7. The TDOS and PDOS spectra of the doped HexGALs by (a) boron and (b) nitrogen. The black upward and red downward lines in TDOS represent spin-up and spin-down states, respectively. The cyan upward and pink downward lines in PDOS represent spin-up and spin-down states of Pz orbital electrons, respectively. Other colors in PDOS represent the spin-polarized states of other orbital electrons. The positions of labeled atoms are marked in Fig. 6. (For interpretation of the references to color in this figure legend, the reader is referred to the web version of this article.)

respectively, by boron (a) and nitrogen (b). From the PDOS spectra, it can be seen that the states near the bottom of conduction band and the top of the valence band are all occupied by π electrons of all atoms, and boron and nitrogen are no exception, which implies that the π conjugation network are not interrupted at the doping site. Moreover, the states near fermi level are also distributed mainly on the α -carbon atoms when we denote the sublattice of the doping site as β .

4. Conclusion

In conclusion, using first-principles calculations, we investigated the electronic properties of the chemisorption HexGALs by carboxyl and amino, the vacancy defected HexGALs by removing the carbon atoms and the doped HexGALs by boron and nitrogen substitutionally. The chemisorption of carboxyl and amino on HexGALs would make a transition from nonmagnetic semiconductor to magnetic semiconductor in the case of imbalance adsorption on two sublattices, and the calculated magnetic moment is $|n_\alpha - n_\beta| \mu_B$, in which n_α and n_β are, respectively, the carbon number of two sublattices in the π conjugation network. These properties of chemisorption HexGALs are very similar with the case of corresponding vacancy defected HexGALs. However, the energetically favorable site of the second carboxyl or amino adsorption on HexGAL is the site that would eliminate the sublattice imbalance and thus kills the magnetism of the system. On the contrary, the boron and nitrogen doped HexGALs cannot give rise to magnetism because the substitutional doping cannot interrupt π conjugation network at the doping site, thus can achieve p-type and n-type semiconductors, respectively. These results are fairly helpful to the in-depth comprehension of GAL's physics and quite important to the application of GAL on electronic and optical devices.

Acknowledgments

This work was supported by the National Natural Science Foundation of China (Grant nos. 20973013/B030304 and 20973016/B030901), the China Postdoctoral Science Foundation (Grant no. 20090460145) and the Science Develop Foundation of Central South University (Grant nos. 08SDF02 and 09SDF09). We thank Prof. ZhiRong Liu in the College of Chemistry and Molecular Engineering of Peking University for his valuable help.

References

- [1] K.S. Novoselov, A.K. Geim, S.V. Morozov, D. Jiang, Y. Zhang, S.V. Dubonos, I.V. Grigorieva, A.A. Firsov, *Science* 306 (2004) 666.
- [2] A.K. Geim, K.S. Novoselov, *Nat. Mater.* 6 (2007) 183.
- [3] L.A. Ponomarenko, F. Schedin, M.I. Katsnelson, R. Yang, E.W. Hill, K.S. Novoselov, A.K. Geim, *Science* 320 (2008) 356.
- [4] Melinda Y. Han, Barbaros Özyilmaz, Yuanbo Zhang, Philip Kim, *Phys. Rev. Lett.* 98 (2007) 206805.
- [5] Xiaolin Li, Xinran Wang, Li Zhang, Sangwon Lee, Hongjie Dai, *Science* 319 (2008) 1229.
- [6] Dmitry V. Kosynkin, Amanda L. Higginbotham, Alexander Sinitskii, Jay R. Lomeda, Ayrat Dimiev, *Nature (London)* 458 (2009) 872.
- [7] Li Liying Jiao, Xinran Zhang, Georgi Wang, Diankov, Hongjie Dai, *Nature (London)* 458 (2009) 877.
- [8] Yuanbo Zhang, Tsung-Ta Tang, Caglar Girit, Zhao Hao, Michael C. Martin, Alex Zettl, Michael F. Crommie, Y. Ron Shen, Feng Wang, *Nature (London)* 459 (2009) 820.
- [9] Thomas G. Pedersen, Christian Flindt, Jesper Pedersen, Niels Asger Mortensen, Antti-Pekka Jauho, Kjeld Pedersen, *Phys. Rev. Lett.* 100 (2008) 136804.
- [10] Thomas G. Pedersen, Christian Flindt, Jesper Pedersen, Antti-Pekka Jauho, Niels Asger Mortensen, Kjeld Pedersen, *Phys. Rev. B* 77 (2008) 245431.
- [11] Joachim A. Fürst, Thomas G. Pedersen, Mads Brandbyge, Antti-Pekka Jauho, *Phys. Rev. B* 80 (2009) 115117.
- [12] J.A. Fürst, J.G. Pedersen, C. Flindt, N.A. Mortensen, M. Brandbyge, T.G. Pedersen, A.-P. Jauho, *New J. Phys.* 11 (2009) 095020.
- [13] L. Rosales, M. Pacheco, Z. Barticevic, A. León, A. Latgé, P.A. Orellana, *Phys. Rev. B* 80 (2009) 073402.
- [14] D.A. Bahamon, A.L.C. Pereira, P.A. Schulz, *Phys. Rev. B* 79 (2009) 125414.
- [15] Decai Yu, Elizabeth M. Lupton, Miao Liu, Wei Liu, Feng Liu, *Nano Res.* 1 (2008) 56.
- [16] De-en Jiang, Valentino R. Cooper, Sheng Dai, *Nano Lett.* 9 (12) (2009) 4019.
- [17] J. Eroms, D. Weiss, *New J. Phys.* 11 (2009) 095021.
- [18] T. Gokus, R.R. Nair, A. Bonetti, M. Böhmeler, A. Lombardo, K.S. Novoselov, A.K. Geim, A.C. Ferrari, A. Hartschuh, *ACS Nano* 3 (12) (2009) 3963.
- [19] Michael D. Fischbein, Marija Drndić, *Appl. Phys. Lett.* 93 (2008) 113107.
- [20] Pierre Kuhn, Aurélien Forget, Dangsheng Su, Arne Thomas, Markus Antonietti, *J. Am. Chem. Soc.* 130 (2008) 13333.
- [21] Fangping OuYang, Bing Huang, Zuanyi Li, Jin Xiao, Huanyou Wang, Hui Xu, *J. Phys. Chem. C* 112 (2008) 12003.
- [22] D.W. Boukhalov, M.I. Katsnelson, *Nano Lett.* 8 (12) (2008) 4373.
- [23] Xinran Wang, Xiaolin Li, Li Zhang, Youngki Yoon, Peter K. Weber, Hailiang Wang, Jing Guo, Hongjie Dai, *Science* 324 (5928) (2009) 768.
- [24] Hugo E Romero, Prasoon Joshi, Awnish K Gupta, Humberto R Gutierrez, Milton W Cole, Srinivas A Tadigadapa, Peter C Eklund, *Nanotechnology* 20 (2009) 245501.
- [25] Ke Gang, *Chin. Chem. Lett.* 20 (11) (2009) 1376.
- [26] Ryota Yuge, Minfang Zhang, Mutsumi Tomonari, Tsutomu Yoshitake, Sumio Iijima, Masako Yudasaka, *ACS Nano* 2 (9) (2008) 1865.
- [27] G. Kresse, J. Furthmüller, *Phys. Rev. B* 54 (1996) 11169; G. Kresse, J. Furthmüller, *Comput. Mater. Sci.* 6 (1996) 15.
- [28] J.P. Perdew, K. Burke, M. Ernzerhof, *Phys. Rev. Lett.* 77 (1996) 3865.
- [29] J.P. Perdew, K. Burke, M. Ernzerhof, *Phys. Rev. Lett.* 80 (1998) 891.
- [30] Hendrik J. Monkhorst, James D. Pack, *Phys. Rev. B* 13 (1976) 5188.
- [31] Nobuyuki Shima, Hideo Aoki, *Phys. Rev. Lett.* 71 (26) (1993) 4389.
- [32] L.A. Chernozatonskii, P.B. Sorokin, E. Belova, J. Brüning, A.S. edorov, *JETP Lett.* 84 (2006) 115.
- [33] D.W. Boukhalov, M.I. Katsnelson, *J. Phys.: Condens. Matter* 21 (2009) 344205.